ELSEVIER

Active control of a rod-net formwork system prototype

A. Liew*, Y.R. Stürz, S. Guillaume, T. Van Mele, R.S. Smith, P. Block

Swiss Federal Institute of Technology (ETH), Zurich, Switzerland

ABSTRACT

A prototype rod-net for a fabric formwork system is described, including the fabrication, control of the geometry via turnbuckles, and the measurement of nodal co-ordinates via an image-based theodolite system. Such a net and fabric formwork system consists of a network of tie elements, either discrete or continuous, forming the main falsework structure, onto which is placed a fabric membrane acting as the flexible formwork for the pouring of wet concrete for the forming of a concrete shell. The fabrication of the plastic and steel net components of the prototype is described in detail, including the arrangement of the nodes, rods and boundary conditions. A control system was developed to determine the necessary adjustments at the boundary elements to move the rod-net to a target geometry to eliminate deviations that may arise from fabrication and construction tolerances. This control system showed that with minimal adjustments the rod-net could be directed effectively, resulting in deviations from the target surface reduced from up to 3–9 mm to below 1–2 mm for a 3D rod-net of approximate dimension 2.5 m × 4.5 m × 2.0 m. Additionally, the algorithm provided a more symmetric distribution of deviations around the target. The control system was coupled with 3D point-cloud measurements of markers placed on and around the rod-net by using a motorised image-assisted theodolite and specialised software for spherical and circular targets. This semi-automated process proved to be both efficient and accurate for determining the spatial co-ordinates of the markers and hence the node locations.

1. Introduction

Concrete shells are an efficient structural form, able to cover large spans with minimal structural depth, gaining stiffness through the structure's curvature. Loads can be carried effectively via membrane stresses (in-plane axial stresses) rather than flexural stresses, when the curved geometry is form-found and is resistant to out-of-plane instability. However, it is the curved geometry of many concrete shells that have been built in the past that lead to extensive material use and high labour costs when constructing shells through traditional single-use timber or milled foam formwork. In addition, the structural form can be limited to hypar sections allowing the use of linear falsework and formwork elements in place of more expensive and not reusable milled timber or foam solutions for curved surfaces.

An alternative fabrication method can be found in a net and fabric formwork system consisting of a network of tie elements, either discrete or continuous, forming the main falsework structure, onto which a fabric membrane, acting as the flexible formwork, is placed. The wet concrete is subsequently poured directly onto the fabric, for which the weight of the wet concrete is supported by the net until it has cured into the desired form. Textiles such as Geo-textiles may be used, with a surface finish that can give no adherence of the concrete to the sheet after striking. The net and any supporting falsework and framing may then be removed after the concrete structure is load bearing and then reused to recreate the same structural form.

A history of fabric formwork use for thin concrete shell structures can be found in [1] and [2], including other hyperbolic-paraboloid based cable-net investigations such as [3] and [4], which also described a computational and construction workflow. The prospect of using cable-net formwork for hypar-based bridge crossings can be found in [5]. The use of tensioned formwork alternatives in concrete shell construction could offer a variety of benefits such as 1) a reduced demand on the foundations due to a lower mass of formwork and falsework, 2) promote usable and unobstructed internal space under the system during construction thus avoiding space vacation, 3) encourage formwork re-use for projects with repeated elements, 4) eliminates the material waste experienced with traditional timber formwork and falsework, and 5) open up a more expressive set of double-curved structural forms. Cable-net and fabric based solutions can offer advantages over purely fabric solutions, as the cable elements can be constructed of steel, capable of both spanning greater distances, supporting extra loads, and acting as discrete pre-stressing and control elements. Additionally, a cable-net allows the application of a non-uniform pre-stress state; in a membrane, stresses equalise rapidly after tensioning.

A net formwork system, such as that presented in this research, has great potential in influencing how formwork systems are considered in the construction industry, for the following reasons. All components of the system can be reused either to construct an identical structure or a sub-set of the parts to create a different structure, which leads to effectively zero formwork and falsework material waste. Consequently,

---

there is great economy for fabricating multiple repetitive elements. This is ideal when compared to the material waste involved with milled foam and timber solutions that have heavy carpentry costs. For various structures, especially bridges or construction projects in built-up urban areas, keeping an unoccupied space under the structure can be critical to minimise disturbance. In certain situations, accessibility and logistics would warrant complicated falsework solutions, for example spanning over a river or road

This research project investigates the fabrication, control and measurement of a prototype rod-net formwork system, needed to define a geometrically accurate net such that it will non-uniformly displace under the wet concrete self-weight to cure into the correct final shape.

2. Research methodology

The rod-net's control system comprises of two main components: 1) a control algorithm that calculates which length adjustments are needed to the net in order to keep stresses within safe material limits, and to direct the geometry to a target shape, and 2) a physical system of changing the lengths of prescribed elements, for which threaded turn-buckles have been used in this prototype. This combined algorithmic and physical control system is then applied to make fine adjustments to the geometry of the rod-net, from spatial deviations that may arise from both fabrication and construction tolerances. Such deviations must be corrected before the pouring of the concrete so that the as-built geometry is as close as possible to the design intent.

The control system is coupled with 3D point-cloud measurements of markers placed on and around the rod-net by using expertise and specialist equipment. The measurement of the 3D point-cloud is realised at the sub-millimetre level by the deployment and combination of several QDaedalus systems (using multiple theodolites for improved coverage), taking measurements from underneath the rod-net. The QDaedalus system is based on a motorised image-assisted theodolite and specialised software, allowing precise spatial measurements of spherical or circular targets. The 3D co-ordinates are obtained by a geodetic network adjustment, based on the spatial directions carried out at different locations. The combination of efficient control and measurement systems allows for quick and precise adjustments of a net on-site before pouring.

The rod-net used to demonstrate the formwork system is based on the roof structure of the NEST-HiLo research and innovation unit [6] for the Swiss Federal Laboratories for Materials Science and Technology (Empa), Dübendorf, Switzerland (see the conceptual image of Fig. 1). The project will feature a full construction-scale net and fabric-formed,

thin-shell concrete roof structure. The NEST-HiLo unit is a collaboration between the Institute of Technology in Architecture, represented by the Professorships of Architecture and Structure (Block Research Group BRG) and Architecture and Building Systems (AIS), architectural office supermanoeuvre and engineering firm Bollinger + Grohmann. HiLo is in the domains of lightweight construction and smart, integrated and adaptive building systems [7-10]. On top of the steel cable-net will be placed a geo-textile fabric formwork, CNC cut and positioned accurately with cut-outs at each node and locked-in with a shear connector. The textile will be taut and strong to support the weight of the concrete within each bay, spanning between the ties without excessive sagging (pillowing) as this leads to additional self-weight. As the geo-textile does not stick to the concrete, even without surface treatment, it can be used many times over without loss of performance, and provides a watertight cover on one side of the concrete during curing and gives the soffit a quality finish after striking.

Extending the prototype cable-net formwork systems for anti-clastic shells developed by the Block Research Group, a 1:4-scale prototype system of the NEST-HiLo roof has been under investigation, as part of formalising the control and measurement protocol for the system, as well as investigating the use of a novel rod and ring network instead of continuous cables. Previous research on cable-net and fabric formwork prototypes can be found in [1] and [11] where information can be found on the calculation of the cable-net forces and pre-stress levels needed for such systems, while the computational form-finding methods can be found in [12]. A variety of steps are needed to design a complete net and fabric formwork system including 1) boundary condition considerations, 2) target shell shapes, 3) the mapping of the cable-net to the shell surface, 4) fabric cutting patterns, 5) tributary nodal load allocations and load combination calculations, 6) best-fit optimisation of cable forces during wet concrete loading, and 7) element sizing of the net and the supporting frame. These steps have been performed previously for the scale model prototype, with this paper focusing on the fabrication and control–measurement process.

Difficulties that arise in utilising such a formwork system, and how they have been tackled in this research, can be summarised as follows:

- The model that has been set up to tackle the computational modelling of a tension-only network with a high degree of statical indeterminacy is described in Section 5.2. This model is characterised by an efficient energy minimisation algorithm for finding static equilibrium using the coordinates of the free nodes as variables. This solves for the high indeterminacy of the rod-net, the tension-only condition via appropriate optimisation constraints, and makes the
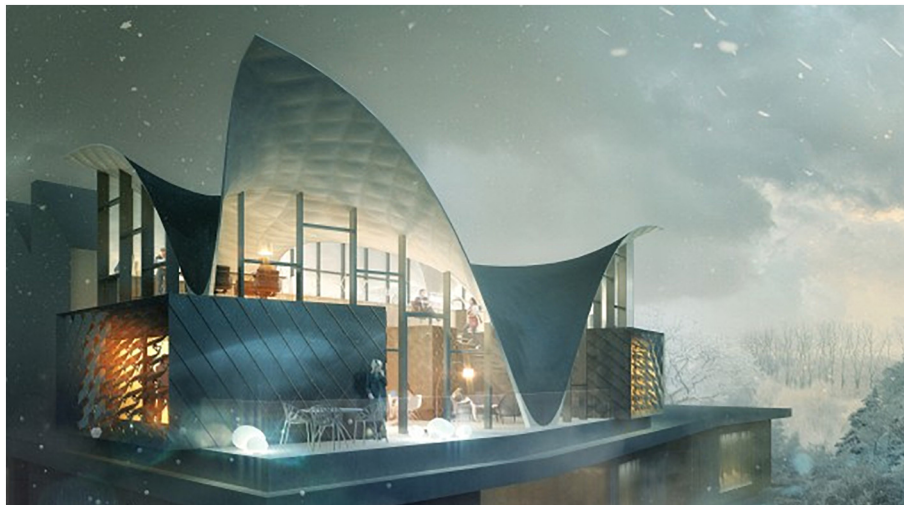

Fig. 1. The NEST-HiLo research and innovation unit at Empa, Dübendorf, CH.
Source: Image: supermanoeuvre/Doug & Wolf.

geometrically complex problem manageable by allowing the free nodes to move in the computational model.

- The sensitivity of the rod-net geometry to deviations from changes in length, either intentional or through fabrication and erection tolerances. This is the problem being tackled in this paper by incorporating the control scheme described later in Section 5.3, which can manipulate the net to achieve a desired geometry. This is performed for the practical construction situation where the as-built geometry is imperfect, which is simulated in our prototype. We will see later in Section 6 the magnitude of the improvements that can be found by applying this control scheme to the 1:4 scale prototype.

- Appropriately detailing components such as the framework and nodes for strength, ease of assembly and allowing the necessary local rotations of the connecting rods. These properties of the rod-net prototype will be explained throughout Section 3 when describing the construction of the physical model. Special attention was given on providing strong steel nodes that provided all necessary degrees-of-freedom needed by the incoming connecting rods. Forces were controlled with a combination of load cells and turnbuckles to keep the rod deformations elastic, and the tension loads to levels that would not deform the timber frame and affect the geometry of the rod-net through falsework movements.

- The final challenge is the one emphasised in this paper, with the intention that such control methods demonstrated on small-scale prototypes can be extended and applied on-site with construction-scale formwork and structures. This prototype forms the first 1:4 scale model of a system that is to be used on a larger construction scale for the same double-curved geometry. This allows us to develop the control system on a cost-effective and meaningful scale, and then to learn from the results and make refinements to both the digital methods and the construction and fabrication details of the rod-net. This combination of small-scale validation and improvements, is important to develop the system for use in construction as an alternative formwork method for concrete construction.

The cable-net geometry is based on a funicular network, that in its pre-stressed state, is a tension-only steel tie structure. Stiffness is gained through the geometry, via the double-curvature of the structure, allowing the cable-net to be lightweight and still efficiently take external loading. The design external loads were used in a force density analysis, where the force densities of the cable elements (the forces divided by the lengths) were defined, and the equilibrium of the structure found through a form-finding process to create the geometry, subject to a best-fit algorithm and a target design shape.

This paper details the construction and properties of the rod-net scale model in Section 3, the measurement process and equipment used to determine the geometry of the rod-net in Section 4, and the control algorithm used to determine which boundary turnbuckles were adjusted for a given target shape in Section 5, followed by the results and conclusions in Section 6 and Section 7, respectively. These sections describe the complete process summarised in Fig. 2.

3. Physical model

This section shows the physical and plan layout of the rod-net in Section 3.1, describes the node detail in Section 3.2, the rods that were used in Section 3.3, the boundary turnbuckles and supporting wooden frame in Section 3.4, and finally the load cells used at the net corners in Section 3.5.

3.1. Layout

The prototype consisted of steel ring nodes connecting plastic rods to form a net structure. This was fastened to a timber housing via turnbuckles at fixed boundary points. The rod-net geometry was adjusted by tightening selected turnbuckles and recording the resulting nodal displacement field via spherical and circular markers at key locations across the net, as well as through force changes in load cells positioned at the net's four corner points. The completed rod-net can be seen in Fig. 3 with a plan layout in Fig. 4. The overall dimensions are approximately 2.5 m × 4.5 m × 2.0 m.

3.2. Nodes

There were a total of 370 nodes, of which 75 were fixed nodes connected to the boundary timber frame and constrained from translating in all directions, and 295 internal nodes that were free to displace as the turnbuckles were adjusted. A photo of one of the internal nodes is shown in Fig. 5 and can be described by the following components: 1) a steel ring, either small, medium or large depending on the number and type of rods entering the junction, 2) the incoming rods, which could slide around the ring and whose intersection formed the nodal point, 3) black and white circular markers at the ends of the larger rod forks and black spherical markers at the end of smaller rods, and 4) 3D-printed white plastic spacers added to the ends to avoid the elements sliding up and down a pin. Small steel rings were used for most nodes, with medium sized rings used to connect some of the larger rods, and three large rings at the key large rod junctions, where forces were larger and more elements connected together. The location of all of the rings can be seen in the plan view of Fig. 4.

3.3. Rods

The prototype consisted of 606 rods, mainly of small diameter (3.24 mm) except for the net spine and the vertical elements connected to the wooden supports. This is where the forces were higher and so larger diameter rods (6.62 mm) were used. The layout of the different rod types is shown in Fig. 4. Each element was a threaded Polyamid PA6 element with a spherical marker at each end to allow measurements of strains by recording changes in length. A steel fork head allowed connection to the node ring via a pin. The nominal unstressed lengths were given for each rod based on a digital model of the net structure, and then cut and fixed to these lengths as close as possible by measuring with a calliper micrometer. When it was not possible to place a small plastic rod in-between nodes, small metal screws were used instead, these are marked as the small internal blue elements in Fig. 4. The rods and nodes form chains that spans continuously across the timber framing from one side to the other. Although no concrete was poured after the control sequence testing, rods were spaced in this system so that concrete pockets would not sag fabric excessively between supporting net lines, and not too close that fabrication became too complex.

3.4. Boundary perimeter

Connection of the net to the boundary timber frame took place via the steel turnbuckles shown in Fig. 6. Each turnbuckle connected to the end of a terminating plastic rod and with a steel bolt-nut-ring combination located at the timber frame. These elements around the net periphery are marked in blue in Fig. 4. Only a single rod and turnbuckle was connected to a fixed boundary node; hence, there are 75 boundary rods for each of the 75 boundary nodes. The turnbuckles that were used, had a displacement range of 50 mm, and so the net was placed in a starting configuration in the middle of this range, allowing a control of ± 25 mm via extension or shortening measurements by a calliper micrometer.

The wooden frame as seen in Fig. 7 performed the function of providing anchorage to the tie forces at the perimeter of the net. This would take the form of steel profiles supported by braced scaffolding, for example, in construction projects for both re-usability, strength and stiffness. The frame must be able to withstand both the expected prestressing loads from the net (deriving from the net and subsequent
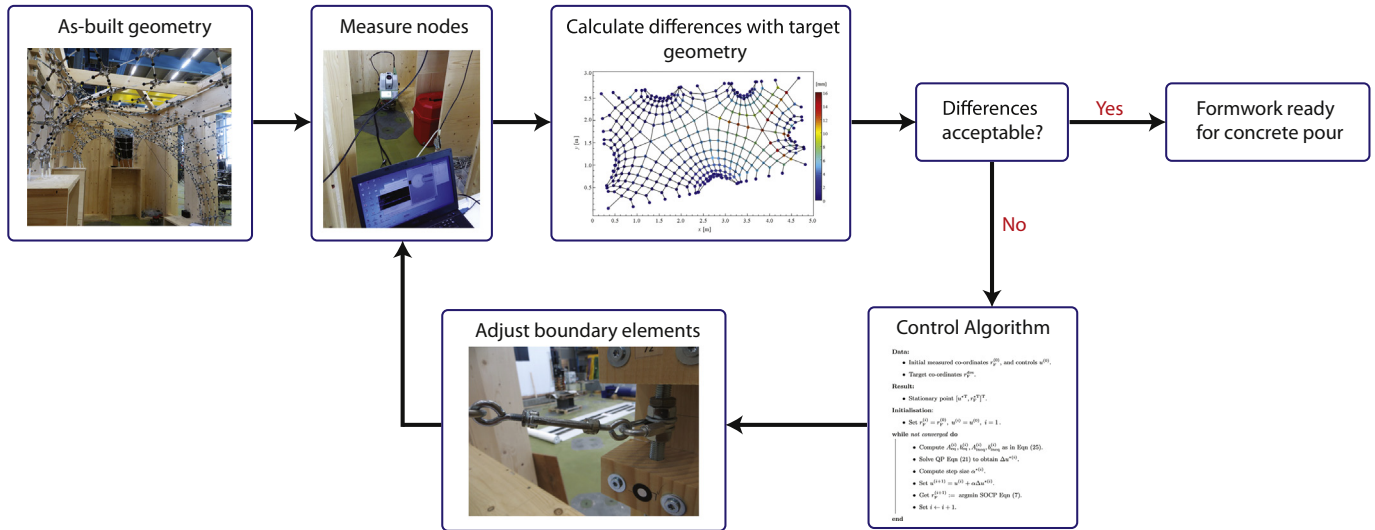
Fig. 2. Overview of the construction, measurement, control and feedback loop, for controlling the geometry of the rod-net.
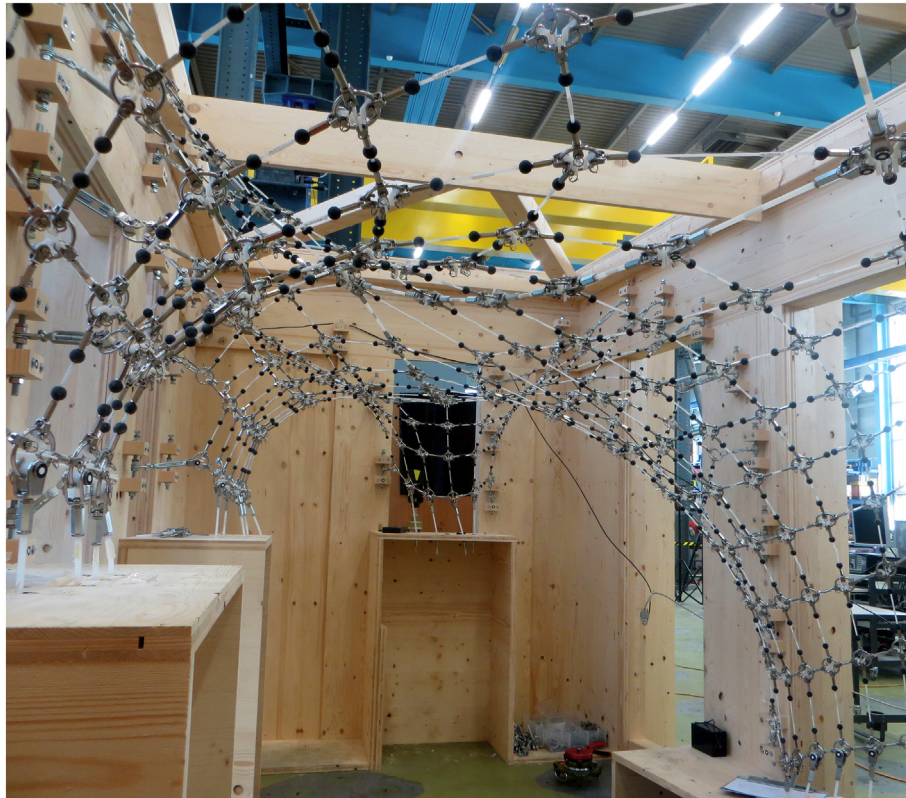

Fig. 3. Complete net structure inside the timber housing.

concrete pour), and not deflect so that the pinching together of the boundary distorts the shell geometry. Frame stiffness was identified as an important parameter in previous studies without control [11]. To check the deflections of the timber housing, circular stickers were placed on the boundary points and measured during the sequencing stages (Fig. 6). It was found that only small deflections occurred in this setup (see later in Section 4.1.4).

3.5. Load cells

Four Zemic S-type 1.5 kN load cells were placed at the four corner boundary locations to measure forces passing through the corner rods

during the control stages (these load cells are shown in Fig. 8). A direct in-line connection and force reading was preferred to a device branching over the corner rods and acting in parallel, as the measurements would need to be corrected based on the relative rod and device stiffness. The load cells allowed the recording of the forces before and after the tightening of turnbuckles, to keep forces as low as possible and within the elastic range of the rods. From material tests on the large rods that connected to the load cells, it was determined that the material stress–strain curve showed an approximately linear behaviour with Young's modulus $E = 1650$ MPa up until 25 MPa, which is equivalent to a force of 860 N in the rods. The initial corner rod forces were between 130 N and 170 N, and then throughout the sequencing
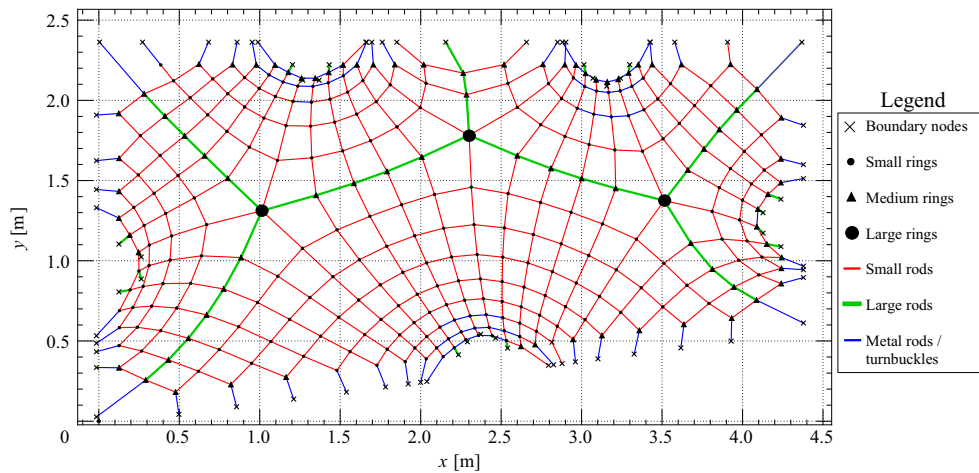
Fig. 4. Layout of the prototype's cable-net setup. (For interpretation of the references to color in this figure legend, the reader is referred to the web version of this article.)

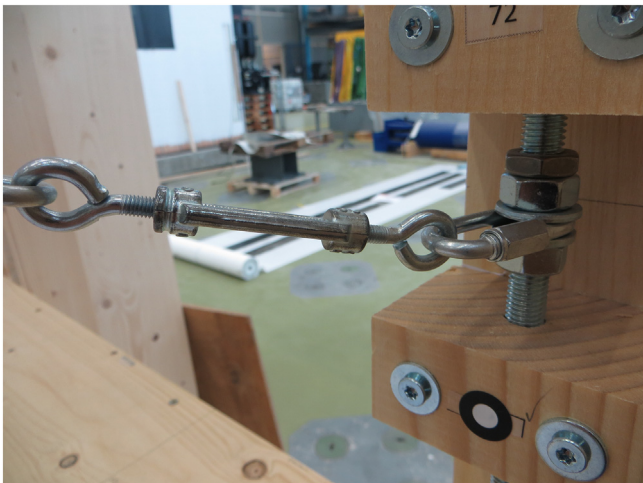**Fig. 5.** Node setup, consisting of ring, rods, markers and spacers.

Fig. 6. Boundary connector setup with small steel turnbuckle.

described in Section 3.6, the forces remained below 415 N, less than half the determined yield load. The full-scale structure's cable-net will take tensile forces up to around 50 kN along the main spine at the corners, where the force magnitudes are dominated by the pre-stress load, and not the self-weight loads of the incoming concrete pour. The 1:4 scale prototype described in this paper takes much more modest

forces of less than 0.5 kN, to keep the internal stresses within the elastic range of the materials. It was observed that the recorded forces picked-up by the load cells, were within about 10% of the expected values.

3.6. Sequences

Each measurement sequence was given an epoch number from 0 to 7, with 0 being the as-built net structure. During each epoch, all spherical and circular markers' co-ordinates were recorded, with the differences between each epoch related to how much each selected boundary turnbuckle was adjusted. The amount that a specific turnbuckle was adjusted was based on the control algorithm described in Section 5. Here, the epochs are summarised with the aid of Fig. 9 to show which and by how much each turnbuckle was adjusted for each epoch stage.

- **Epoch 0**: This was the initial configuration or as-built base state. The turnbuckles all lay approximately in the centre of their adjustable range and the net was taut.
- **Epoch 1**: A movement of the net to the right via the shortening of the turnbuckles located at (1): 20.0 mm, (2): 16.0 mm and (3): 21.6 mm (blue circles in Fig. 9). This increased the forces in the rods connected to (1) and (3) by 133% and 85% respectively, while also increasing the rod forces at the other side by (4) 20% and (6) 25%.
- **Epoch 2**: Release of the net from Epoch 1 back to the base state Epoch 0, by reversing (1), (2) and (3) from Epoch 1, i.e lengthening (1): − 20.0 mm, (2): −16.0 mm and (3): −21.6 mm.
- **Epoch 3**: A movement of the net to the left via the shortening of the turnbuckles located at (4): 20.5 mm, (5): 8.4 mm and (6): 19.5 mm (red circles in Fig. 9). This increased the forces in the rods connected to (4) and (6) by 137% and 173% respectively, while also increasing the rod forces at the other side by (1) 32% and (3) 28%.
- **Epoch 4**: The net was moved back to Epoch 0, ready for subsequent control stages for which the turnbuckles at the orange circles in Fig. 9 were then also used.
- **Epoch 5**: The target geometry was that of the previous Epoch 2, which ensured that the control algorithm was focused on finding the turnbuckle adjustments needed for a net configuration that can be physically obtained within the ± 25 mm turnbuckle range. The following points were adjusted: (1): 12.6 mm, (2): 9.0 mm, (3): 13.2 mm, (7): 7.4 mm and (8): 5.5 mm.
- **Epoch 6**: The net was then pulled again to the left (Epoch 3), thus the turnbuckles needed to remove the net pulling the right as well as the changes needed to move to the left. These were as follows: (1): − 17.0 mm, (2): −4.2 mm, (3): −15.8 mm, (7): −7.4 mm, (8):

Fig. 7. A stiff wooden frame provided the anchorage for the boundary rods and data a logger measured forces in the corner rods.
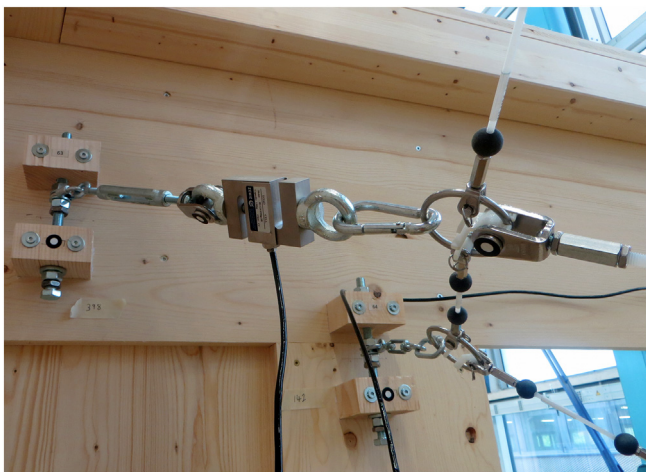

Fig. 8. Corner load cells measured forces in the rods of the main spine (highlighted green in Fig. 4).
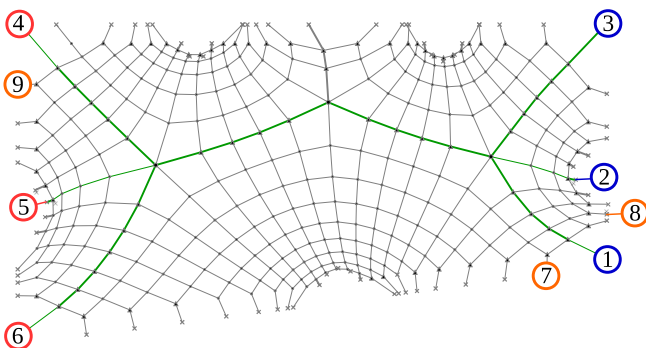

Fig. 9. Boundary nodes that were changed as part of the sequencing stage for different epochs. (For interpretation of the references to color in this figure legend, the reader is referred to the web version of this article.)

−5.5 mm, (4): 2.9 mm, (5): 8.6 mm, (6): 6.8 mm and (9): 5.5 mm.
- **Epoch 7**: The final epoch involved the following movements: (1): 5.2 mm, (2): −7.5 mm, (3): 2.2 mm, (4): 16.5 mm, (5): −0.3 mm,

(6): 13.2 mm and (9): −3.3 mm.

4. Measurements

This section provides the information on the QDaedalus equipment and how the point cloud data was retrieved in Section 4.1 and Section 3.6 gives a description of the eight point-cloud snapshots (Epoch 0 to Epoch 7).

4.1. QDaedalus

The 3D positions of the markers were obtained by the triangulation of spatial directions (geodetic network). The directions were measured by the image-based theodolite system QDaedalus [13,14]. Among all available techniques to date, this system was chosen for a variety of reasons. The main reason was to deploy a system that could provide absolute co-ordinates with sub-millimetre accuracy not only for the 1:4-prototype presented in this paper, but also for the final 1:1 HiLo NEST roof formwork. In addition, due to the high density and the number of markers that needed to be determined (~1000), it was also crucial to have a system that gave the possibility to find a balance between the level of automation and the reliability of the data acquisition.

4.1.1. System description

The QDaedalus system has been developed at the Institute of Geodesy and Photogrammetry of ETH Zurich and consists of both hardware and software components. The hardware portion is composed of a commercial motorised Leica total station (for this project the TS60 series, as shown in Fig. 10) on which a modified industrial CCD camera is inserted in place of the eyepiece. The system provides a field-of-view of 1° and a resolution of 4 arcsec per pixel, which corresponds to a lateral resolution of 0.2 mm for an object at a distance of 10 m. The accuracy (1σ) varies between 0.1 pixel (0.02 mm/10 m) for optimal automatic target extraction, and 2 pixels (0.4 mm/10 m) for manual picking.

4.1.2. Measurement stages

The stages that were needed for the data acquisition of a single station, began with the set-up of the QDaedalus system at an arbitrary location. Following this stage, the co-ordinates of the station were
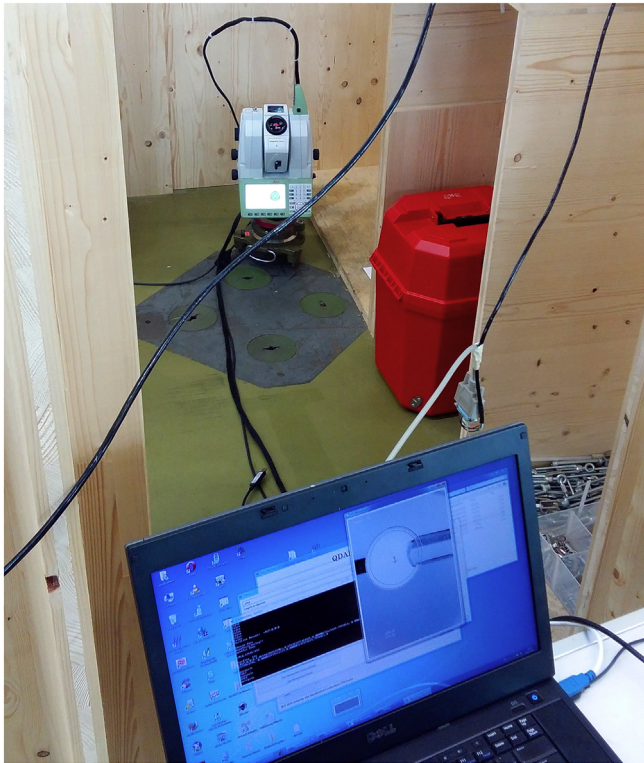
Fig. 10. The QDaedalus system consists of both hardware (Leica total station) and software components.
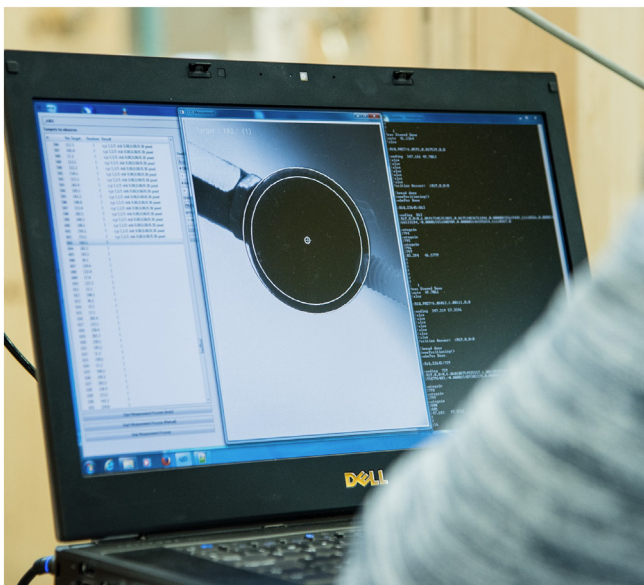

Fig. 11. Semi-automatic measurement of a spherical marker.

determined by a free-station procedure. Then, by using the approximate co-ordinates of all markers (given by the previous epoch), the total station was sequentially pointed towards the approximate direction of each of the markers. At this stage, the current marker was visible in the field-of-view, and the QDaedalus software attempted to extract automatically the position of the marker in the image and display its solution in the current image. For circular 2D markers, an ellipse matching algorithm was used [15], while for the spherical markers, a circle matching scheme was chosen [13] (a photograph of the circle matching is in Fig. 11). The human operator can accept, reject, or modify directly the extracted position in the displayed image. It is important to notice
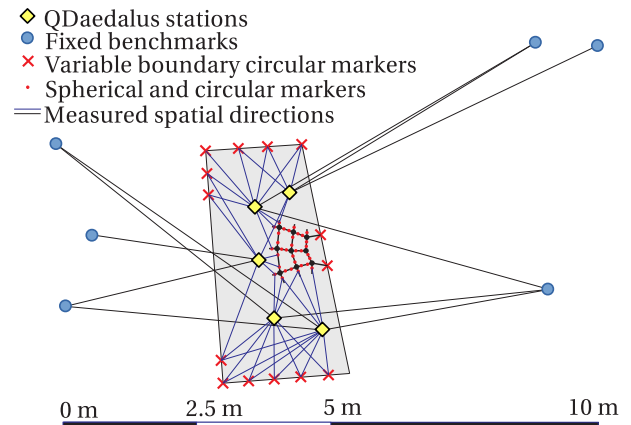

Fig. 12. Overview of the geodetic network.

that for spherical markers the manual picking is very efficient, since the apparent circle can be accurately predicted and integrated into the image, which permits one to precisely measure the direction of spherical markers, even those that are almost fully hidden by other objects.

4.1.3. Measurement strategy

At each epoch measurement, the aim was to determine the absolute position of all markers on the net and those placed on the wooden boundary structure (markers close to the boundary nodes). To achieve this, six circular markers were fixed outside of the wooden frame on stable frameworks. These fixed benchmark points precisely provided the stable (global) reference frame for all epochs (Fig. 12). In a first step, the co-ordinates of the six fixed benchmarks were determined using a classical geodetic network with sub-millimetre accuracy. Then, for each epoch, the measurement strategy consisted of measuring the spatial directions of all visible markers from five QDaedalus stations located inside the boundary perimeter. This represents approximately 9000 single angular observations for the determination of approximately 950 points (or 2850 co-ordinates). The measurements were completed in a total of 12.5 h, or 6.25 h with two stations working in parallel. The co-ordinates of the points for the different epochs were computed separately, with only the six benchmark points considered as fixed. The QDaedalus station's co-ordinates and all other markers were considered as unknown variables. The computations were performed with the geodetic software TRINET+ [16]. The mathematical model of TRINET+ is based on a rigorous 3D observation equation model and affords a weighted least-squares adjustment. In addition, to quantify the quality of the observations and the co-ordinates, TRINET+ provides all standard state-of-the-art geodetic statistical indicators.

4.1.4. Boundary stability

The stability of the wooden structure was analysed using the displacement vectors of markers on the boundary between the different epochs. The statistics of the norm of the vectors are listed in Table 1. It

Table 1
Statistics of the displacements at boundary markers [mm]. Standard deviation (std) and root-mean-squared (rms).

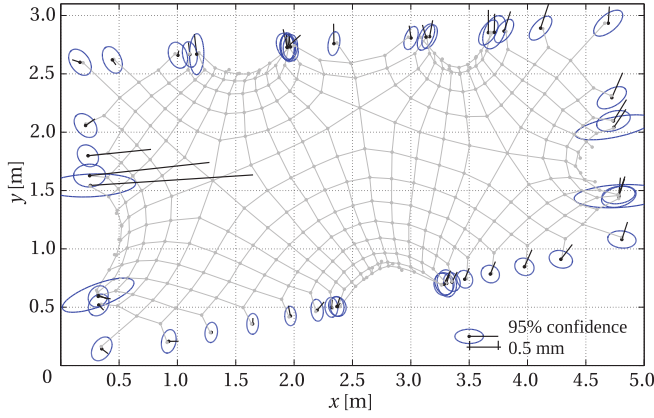| Epochs	Min	Max	Std	rms
0–1	0.04	2.79	0.46	0.58
1–2	0.12	0.60	0.10	0.31
2–3	0.24	0.76	0.14	0.50
3–4	0.31	0.69	0.09	0.49
4–5	0.16	0.70	0.15	0.39
5–6	0.03	1.14	0.23	0.62
6–7	0.06	0.98	0.23	0.59
1–7	0.05	0.61	0.11	0.22

Fig. 13. Displacement vectors between Epoch 0 and Epoch 1 and the confidence ellipses (95% confidence level).

is seen that the largest displacements were observed between Epoch 0 and Epoch 1 (Fig. 13).

As we can see in Table 1, only three points were subjected to displacements larger than 1 mm, with the other points mostly below statistical significance and did not exceed 0.4 mm. Concerning the stability of the markers on the boundary between Epoch 1 and Epoch 7 in Fig. 14, we can conclude that the root-mean-squared and the standard deviation of the displacements are approximately 0.45 mm and 0.15 mm, respectively.

4.1.5. Determination of the displacements

The displacements of the nodes were not directly measured, but were derived from the displacements of the markers attached to the rods, as in Fig. 15.

The precision of the node displacement readings were assumed to be similar to the empirical precision of the markers. In Fig. 16, the 95% empirical confidence ellipses show that the horizontal precision of almost all markers are isotropic. In addition, the histogram and the empirical cumulative distribution function of the 95% major semi-axis (Fig. 17) shows that the accuracy (95%, with respect to the fix benchmarks) of almost all points was below 0.4 mm.

5. Control algorithm

This section describes how the geometry of the net was controlled. First, a motivation and the principle of the control scheme are given in Section 5.1. This is followed by the mathematical model of the net in Section 5.2, and finally, the control algorithm in Section 5.3.
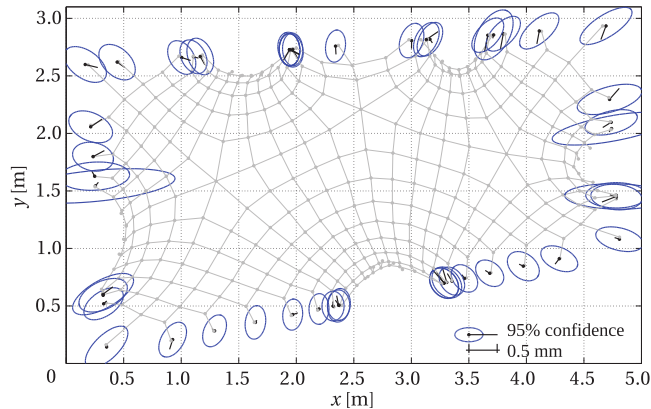

Fig. 14. Displacement vectors between Epoch 1 and Epoch 7 and the confidence ellipses (95% confidence level).

5.1. Motivation and principle of control

It is important to fabricate precisely the intended geometry of the shell, as it is optimised for the shell's engineering design and its stability or buckling behaviour. Furthermore, other elements such as the facade, may need to adhere to tight tolerances. Because of fabrication and construction tolerances and other uncertainties such as the actual material properties and behaviour, it can never be guaranteed that the required precise fit is achievable if the construction process is open-loop, which is the state-of-the-art. Open-loop means that there is no detection and systematic correction of errors during the construction.

The presented approach transforms the open-loop construction to a closed-loop methodology, where, after the initial construction, a closed-loop is implemented by iteratively measuring and correcting the as-built geometry. This is done by measuring the deviations from the desired geometry and using the information to compute which adjustments are needed to bring the geometry closer to the desired case, and thus decreasing the error in the construction. The control algorithm, which is used for steering of the net geometry to the desired target shape, is model-based. This means that the computation of the control inputs is based on the knowledge of how the system behaves.

5.2. Net model

Details about the model parameters of the net's control algorithm are summarised here, with further details found in [17]. One defines the geometry of the system by the co-ordinates of the nodes, which are denoted as

$$x = [x_\mathrm{F}^\mathrm{T}, \quad x_\mathrm{B}^\mathrm{T}]^\mathrm{T}, \quad y = [y_\mathrm{F}^\mathrm{T}, \quad y_\mathrm{B}^\mathrm{T}]^\mathrm{T}, \quad z = [z_\mathrm{F}^\mathrm{T}, \quad z_\mathrm{B}^\mathrm{T}]^\mathrm{T} \in \mathbb{R}^n, \quad (1)$$

where x_F, y_F, $z_\mathrm{F} \in \mathbb{R}^{n_\mathrm{F}}$ represent the co-ordinates of the free nodes, which lie in the inner region of the rod-net, and the co-ordinates x_B, y_B, $z_\mathrm{B} \in \mathbb{R}^{n_\mathrm{B}}$ collect the nodes of the boundary, which lie on the supporting frame. The free nodes and the boundary nodes are visualised in Fig. 4, together with their realisations in the prototype as small, medium and large rings or as anchor points on the wooden frame. One stacks the x, y and z co-ordinates of the single nodes together and denote them by $r_\mathrm{s} = [x_\mathrm{s}, y_\mathrm{s}, z_\mathrm{s}]^\mathrm{T}$ for the nodes s. Similarly, we define the stacked vectors $r_\mathrm{F} = [r_1^\mathrm{T}, ..., r_{n_\mathrm{F}}^\mathrm{T}]^\mathrm{T}$, $r_\mathrm{B} = [r_{n_\mathrm{F}+1}^\mathrm{T}, ..., r_n^\mathrm{T}]^\mathrm{T}$ and $r = [r_\mathrm{F}^\mathrm{T}, r_\mathrm{B}^\mathrm{T}]^\mathrm{T}$, containing the co-ordinates of all free, all boundary and the collection of all co-ordinates of the net, respectively.

Parameters of the system are given by the material properties of the single edges, denoted by $EA_{(\mathrm{s},t)}$, representing the product of the Young's modulus E and the cross-section area A of the edge (s,t). Fig. 4 shows the different materialisations of the edges of the net. Further fixed parameters of the system are the unstressed lengths of the edges, denoted by the vector $l_0 = [l_{0,1}, ..., l_{0,m}]^\mathrm{T}$. For the interior edges, these lengths cannot be changed once the rod-net is constructed. However, the boundary edges of the net connect to the wooden frame via the described turnbuckles, which can introduce a defined change in length. We define this possible change in length for all edges as the vector of control inputs

$$u := [u_1, ..., u_m]^\mathrm{T} \in \mathbb{R}^m, \quad (2)$$

with

$$u_{(\mathrm{s},t)} := \begin{cases} \Delta l_{0,(\mathrm{s},t)} & \text{if}(\mathrm{s}, t)\text{ is a boundary edge,} \\ 0 & \text{if}(\mathrm{s}, t)\text{ is a free edge.} \end{cases} \quad (3)$$

We define the length of edge (s,t) after applying the control input as $\bar{l}_{0,(\mathrm{s},t)} = l_{0,(\mathrm{s},t)} - u_{(\mathrm{s},t)}$. These possible adjustments in the lengths of the boundary edges are used to steer the geometry of the net as close as possible to the target shape. However, determining how to change the lengths is not trivial. For the prototype, the 75 boundary edges of the net give 10^{22} possible combinations of cable adjustments, and this is without deciding how much to adjust each edge. The control algorithm
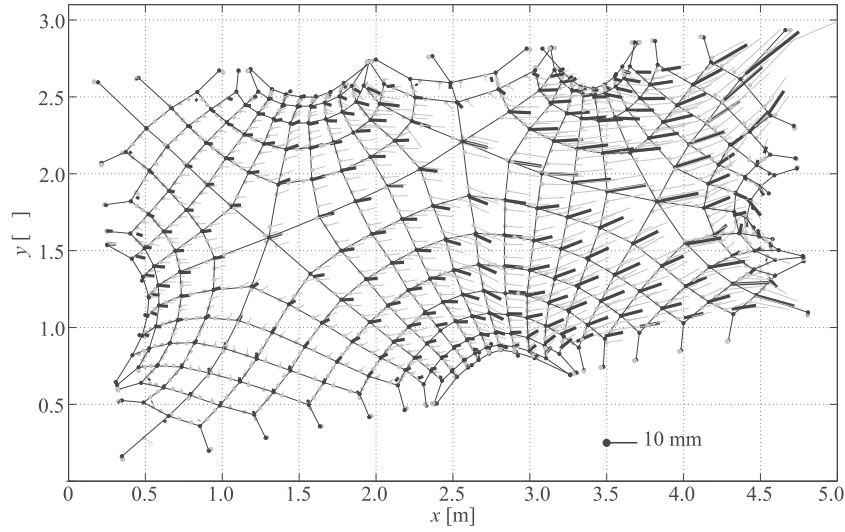
Fig. 15. Horizontal displacements of the markers (grey) and nodes (black) between Epoch 0 and Epoch 1.

is required to compute the vector of control inputs u to be applied to the turnbuckles.

The target state is a desired static configuration of the net; therefore, the model-based control algorithm makes use of a characterisation of the static equilibria of the net. This characterisation can be given by two equivalent formulations [17]. One consists of the force balances in the x, y, and z directions at the free nodes. For free node s, these three force balances are given by

$$h_s := \sum_{t \in \mathcal{N}_s} \left[(r_s - r_t) \left(\frac{1}{l_{0,(s,t)} - u_{(s,t)}} - \frac{1}{l_{(s,t)}} \right) EA_{(s,t)} \right] = 0 \in \mathbb{R}^3, \tag{4}$$

$$\forall\, s \in \mathcal{N}_N \tag{5}$$

where we denote by $\mathcal{N}_s$ the set of neighbouring nodes of node s, and $l_{(s,t)}$ is the length of the edge (s,t), given by

$$l_{(s,t)} := \|r_s - r_t\|_2. \tag{6}$$

The second formulation of equilibria configurations is given by the following second-order cone optimisation program, which has been proposed in [18] for a similar problem:
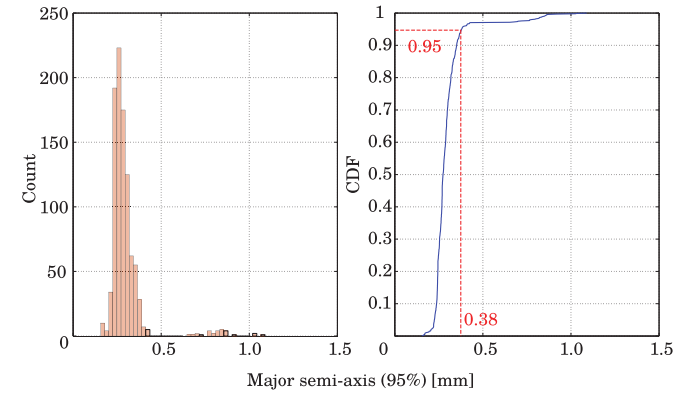
$$\min_{r_F, w, v} \frac{EA}{2} v \tag{7}$$

Fig. 17. Histogram and empirical cumulative distribution function (CDF) of the major semi-axis of the 95% confidence ellipses of all markers, for a specific epoch.

$$\text{s.t.} \frac{\|r_s - r_t\|_2 - (l_{0,(s,t)} - u_{(s,t)})}{\sqrt{l_{0,(s,t)} - u_{(s,t)}}} \leq w_{(s,t)}, \tag{8}$$

$$0 \leq w_{(s,t)}, \quad \forall\, (s, t) \in \mathcal{E}, \tag{9}$$
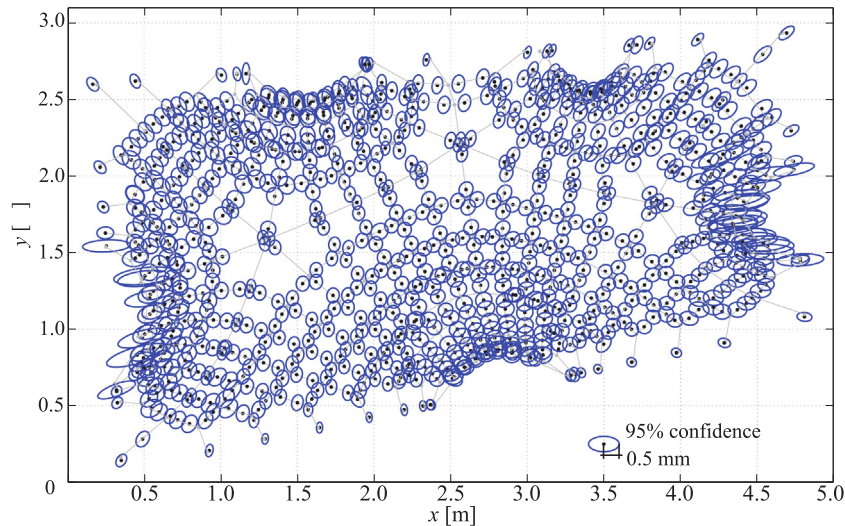

Fig. 16. Confidence ellipses (95% confidence level) of all markers for a specific epoch.

$$\left\| \begin{bmatrix} 2w \\ 1 - v \end{bmatrix} \right\|_2 \leq 1 + v, \tag{10}$$

$$r_B = \bar{r}_B, \tag{11}$$

where $\bar{r}_B$ are the constant co-ordinates of the fixed boundary nodes. The co-ordinates of the free nodes, r_F, of the net in static equilibrium are the minimisers to this optimisation problem.

5.3. Control algorithm

To compute the vector of control inputs to be applied to the system, the following optimisation problem is solved within the control algorithm

$$\min_{r_F, u} \| (r_F - r_F^{des}) \|_{Q_r}^2 \tag{12}$$

$$\text{s.t.} h_s(r_F, u) = 0 \quad \text{for all free nodes s,} \tag{13}$$

$$g_{(s,t)}(r_F, u) \leq 0 \quad \text{for all edges(s, t),} \tag{14}$$

$$u_{lb} \leq u \leq u_{ub}, \tag{15}$$

where the cost function is the weighted L_2-norm of the errors between the as-built, co-ordinates r_F and the desired r_F^{des}, with a weighting matrix Q_r. Furthermore, u_{ub} and $u_{lb} \in \mathbb{R}^m$ represent bounds on the input given by the construction limits, which are the contraction and extension distances of the turnbuckles. The equality constraints $h_s(r_F, u) = 0$ are as defined in Eq. (4) and represent the force equilibria at all free nodes. The m inequality constraints for all edges (s,t) are defined as

$$g_{(s,t)}(r_F, u) := l_{0,(s,t)} - u_{(s,t)} - \| r_s - r_t \|_2 \leq 0, \tag{16}$$

and allow only for tension forces and elongation, as compression in any of the edges is not permitted in the solution.

The non-linear optimal control problem is solved by a variant of Sequential Quadratic Programming [19], which is a very efficient algorithm for solving non-linear constrained optimisation problems. Furthermore, additional constraints can naturally be included in the problem formulation. In our application, this can be necessary to account for additional restrictions in the construction, for example it might be necessary to include bounds on the maximum tensions in the cables in order not to damage the material. Iteratively, it is approximated as a quadratic program by linearising the equality and the inequality constraints, h and g, respectively, which are the stacked equalities of Eq. (4) and the stacked inequalities of Eq. (16)

$$h := \begin{bmatrix} h_1, ..., h_s, ..., h_{n_F} \end{bmatrix}^T \in \mathbb{R}^{n_F}, \tag{17}$$

$$g := [g_1, ..., g_{(s,t)}, ..., g_m]^T \in \mathbb{R}^m. \tag{18}$$

The quadratic problem solved in each iteration of the Sequential Quadratic Programming framework is given by

$$\min_{\Delta r_F, \Delta u} \| r_F + \Delta r_F - r_F^{des} \|_{Q_r}^2 \tag{19}$$

$$\text{s.t.} A_{eq} \begin{bmatrix} \Delta r_F \\ \Delta u \end{bmatrix} + b_{eq} = 0, \tag{20}$$

$$A_{ineq} \begin{bmatrix} \Delta r_F \\ \Delta u \end{bmatrix} + b_{ineq} \leq 0, \tag{21}$$

with

$$A_{eq} \mid_{(r_F, u)} = \nabla_{r_F, u} h(r_F, u) \mid_{(r_F, u)}, \tag{22}$$

$$b_{eq} \mid_{(r_F, u)} = h(r_F, u) \mid_{(r_F, u)}, \tag{23}$$

$$A_{ineq} \mid_{(r_F, u)} = \nabla_{r_F, u} g(r_F, u) \mid_{(r_F, u)}, \tag{24}$$

$$b_{ineq} \mid_{(r_F, u)} = g(r_F, u) \mid_{(r_F, u)}, \tag{25}$$

with $\nabla_{r_F, u}$ the partial derivatives w.r.t. r_F and u.

The overall control algorithm iteratively solves Eq. (21) for the direction Δu, takes a step size of α in this direction, and then determines the new input $u^+ = u + \alpha \Delta u$. The next feasible point is computed as the solution to the second-order cone program for the fixed input u^+. These iterations are repeated until convergence to a stationary point, which can be checked for local optimality. The steps are summarised in Algorithm 1. For further details on the control algorithm, the reader is referred to [17].

Algorithm 1. Overall control algorithm for the form of the net.

Data:

- Initial measured co-ordinates $r_F^{(0)}$, and controls $u^{(0)}$.

- Target co-ordinates r_F^{des}.

Result:

- Stationary point $[u^{*T}, r_F^{*T}]^T$.

Initialisation:

- Set $r_F^{(i)} = r_F^{(0)}, u^{(i)} = u^{(0)}, i = 1$.

while *not converged* **do**

- Compute $A_{eq}^{(i)}, b_{eq}^{(i)}, A_{ineq}^{(i)}, b_{ineq}^{(i)}$ as in Eqn (25).

- Solve QP Eqn (21) to obtain $\Delta u^{*(i)}$.

- Compute step size $\alpha^{*(i)}$.

- Set $u^{(i+1)} = u^{(i)} + \alpha \Delta u^{*(i)}$.

- Get $r_F^{(i+1)} := $ argmin SOCP Eqn (7).

- Set $i \leftarrow i + 1$.

end

6. Results

In this section, the results from the experimental prototype are presented. In the first phase of measurements in Section 6.1, used to determine the model parameters and to validate the model, while in the second phase of experiments in Section 6.2, the control performance is demonstrated.

6.1. First phase: identification and model validation

The first phase of the experiments was used to determine the model parameters of the system and to validate the model. To this end, two movements of the net were performed to both sides of the prototype to observe the model behaviour from the applied inputs. This corresponds to the measured configurations Epoch 0 through Epoch 4 described in Section 3.6. In this first phase, Epoch 0 to Epoch 4 were chosen to be feasible for applied boundary forces and corresponding tensions in the edges kept within a range. This was to ensure that no elements were slack, while also not too high that the material was overstressed, which would have invalidated the linear elastic material properties assumption.

The initial configuration, Epoch 0, was chosen such that all rods were tensioned so that the turnbuckles lay in the middle of their allowable physical adjustment range. The resulting forces, as verified from the placed load-cells, were at the lower range of the allowed elastic forces. Using the measured nodes' co-ordinates of this initial configuration, $r^{(0)}$, the parameters are chosen as

$$l_{0,(s,t)} = 0.990 \quad l_{(s,t)}^{(0)}, \quad \text{if(s, t)is an extensible edge,} \tag{26}$$

$$l_{0,(s,t)} = 0.999 \quad l_{(s,t)}^{(0)}, \quad \text{if}(s,t)\text{is a stiff metal edge}, \tag{27}$$

where $l_{(s,t)}^{(0)} = \|r_s^{(0)} - r_t^{(0)}\|_2$ is computed from the measured co-ordinates, $r^{(0)}$, of the first configuration, Epoch 0. The stiff edges are those realised as metal rods. This choice of parameters l_0 is based on the following approximation:

$$f_{(s,t)} = EA_{(s,t)} \frac{\Delta l_{(s,t)}}{l_{0,(s,t)}}$$

$$\Rightarrow \frac{\Delta l_{(s,t)}}{l_{0,(s,t)}} = \frac{f_{(s,t)}}{EA_{(s,t)}} = \frac{150 \quad \text{N}}{1650(10)^6 \frac{\text{N}}{\text{m}^2} \pi \, [3.24(10)^{-3} \quad \text{m}]^2} \tag{28}$$

$$= \frac{150 \quad \text{N}}{1.36(10)^4} \approx 0.01. \tag{29}$$

For the extensible small rods, which form the majority of the net elements and model behaviour. The force distribution is assumed to be approximately uniform for the first stage to obtain a strain of ≈ 0.01, which means that the elongation Δl is $\approx 1\%$ of the unstressed length l_0.

6.2. Second phase: control of the form

In the second phase of experiments, two control scenarios were performed, where the goal was to achieve a desired geometry of the net starting from a perturbed configuration. To achieve the desired geometry, the lengths of the boundary edges were adjusted via the turnbuckles according to the output of the control algorithm. Making use of the measured co-ordinates from the first phase of experiments, these configurations were known to be attainable for the system within the acceptable range of rod forces. For the first control scenario, the perturbed starting configuration was Epoch 4. The target form was chosen to be the measured Epoch 1. For the second control scenario, the starting configuration was set to Epoch 5, which was that resulting at the end of the first control scenario. The target configuration was then set to the measured configuration Epoch 3. The following details the results of the first control scenario, which is representative of the control performance, the second control scenario was equally successful.

The output of the control algorithm, Algorithm 1, for the first control scenario from $r_F^{(0)} := r_F^{(\text{Epoch 4})}$ and $r_F^{\text{des}} := r_F^{(\text{Epoch 1})}$ are the alterations in Fig. 9 that result in the configuration Epoch 5. The optimal control problem is solved in Algorithm 1 and is summarised by the following results:

- Cost was decreased by 92.24%, from $\|r^{(\text{Epoch 4})} - r^{(\text{Epoch 1})}\|_{Q_r} = 0.0045$ to a value of $\|r^{(\text{Epoch 5})} - r^{(\text{Epoch 1})}\|_{Q_r} = 3.5212(10)^{-4}$.
- The L_2-norm of the deviations was decreased by 89.94% from $\|r^{(\text{Epoch 4})} - r^{(\text{Epoch 1})}\|_2 = 0.0064$ to $\|r^{(\text{Epoch 5})} - r^{(\text{Epoch 1})}\|_2 = 6.4748(10)^{-4}$.

The histograms in Figs. 18–21 show the absolute, x, y and z deviations in the distance between the node co-ordinates before and after the applied control algorithm, that is from current co-ordinates $r^{(\text{Epoch 4})}$ to changed co-ordinates $r^{(\text{Epoch 5})}$ to get to the desired co-ordinates $r^{(\text{Epoch 1})}$. As the control inputs moved the net mainly along the x-axis, the error is reduced in this dimension, resulting still in a slight influence on the z co-ordinates and least influence on the y co-ordinates.

The results of the first control phase are visualised in Figs. 22 and 23. The figures show the distances from the as-built co-ordinates of the starting configuration before the control, $r^{(\text{Epoch 4})}$ to the desired co-ordinates $r^{(\text{Epoch 1})}$. These deviations are almost completely removed by the control algorithm from $r^{(\text{Epoch 5})}$ to $r^{(\text{Epoch 1})}$.

7. Conclusions

This multi-disciplinary, collaborative project's goal was to use a 1:4-
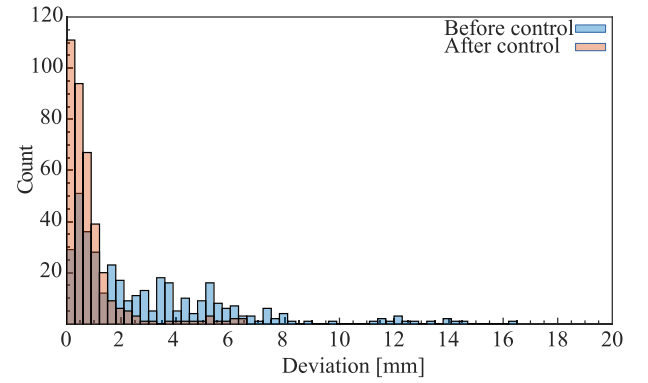

Fig. 18. The magnitude of the deviations from the target surface ranged initially up to around 10–15 mm, and was subsequently reduced to below 2 mm.
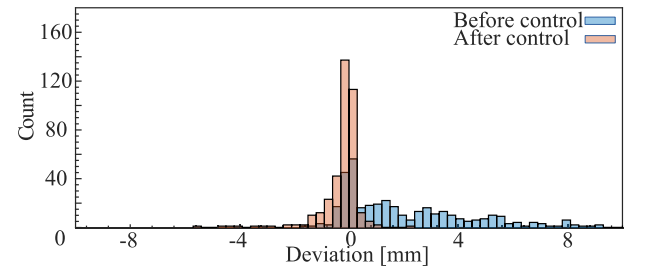

Fig. 19. Most corrections shifted the positive x co-ordinate bias of up to 10 mm to an even distribution of less than 2 mm.
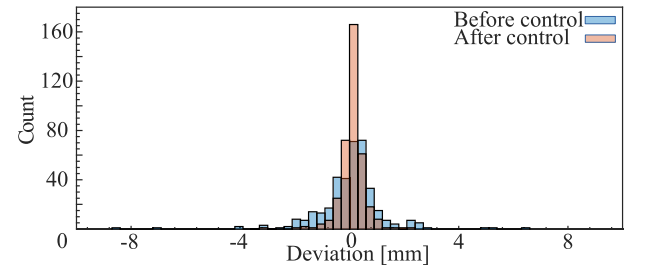

Fig. 20. The y components of the deviations stayed symmetrically distributed, but formed a tighter range around 0 mm, falling from 3 mm to 1 mm.
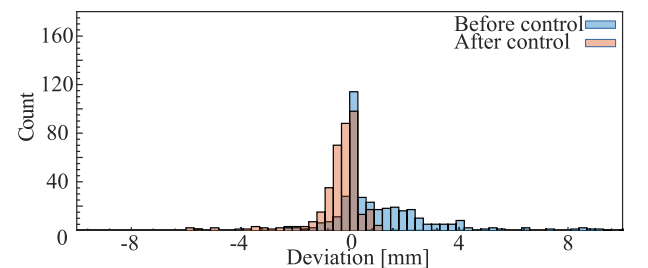

Fig. 21. Improvements in the z co-ordinate deviations also occurred.

scale prototype to inform the 1:1-scale rod-net falsework system of the NEST-HiLo roof. This was to provide valuable data on the fabrication methods and challenges, develop a control algorithm and node measurement process. The following conclusions are made.

The fabrication of the rod-net was described in detail, including the arrangement of the nodes, the rods and the support boundary conditions. The prototype consisted of plastic and steel components controlled by steel turnbuckles at the perimeter, the latter provided a good degree of control over the net geometry.

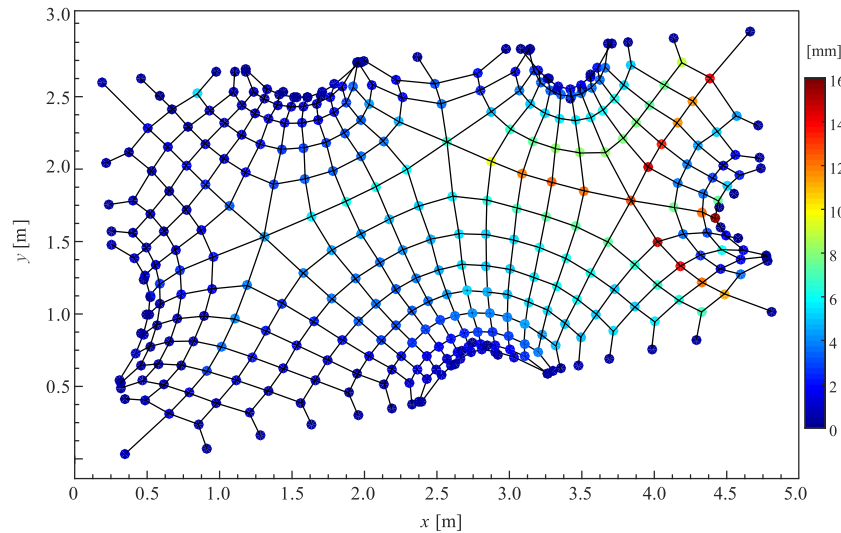The semi-automated QDaedalus measurement process proved to be

Fig. 22. Initial errors: the distance between the as-built co-ordinates before the control $r_s^{(\text{Epoch 4})}$ and the desired co-ordinates $r_s^{(\text{Epoch 1})}$.
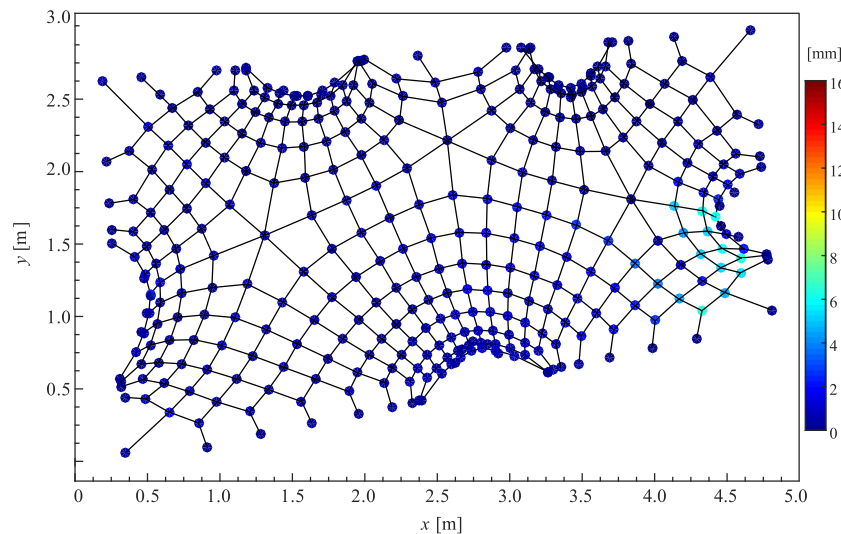

Fig. 23. Controlled errors: the distance between the as-built co-ordinates after the control $r_s^{(\text{Epoch 5})}$ and the desired co-ordinates $r_s^{(\text{Epoch 1})}$.

both efficient and accurate for determining the spatial co-ordinates of the markers and hence the node locations, with the spherical markers proving more effective than the circular stickers. The confidence in the node location estimation reduced somewhat, when it was not physically possible to fit markers symmetrically around a node, leading to less data for a node. For the prototype that was tested, and the number of stations used, there was a good line of sight to all markers as there was no fabric obstruction. For the real construction net, a hanging rod with double spherical markers will be used to form an offset from the fabric surface.

The control algorithm showed that within one to two rounds of turnbuckle adjustments, the net could be directed effectively to a target surface with minimal number of boundary adjustments, as not all turnbuckles were adjusted in between epochs. For the examined 1:4-scale prototype, deviations from the target surface reduced from around 3–9 mm to below 2 mm and gave a more symmetric distribution of deviations. The timber housing used for this experiment was stiff for the magnitude of forces in the rods, but a steel structure would be recommended for larger forces and stiffness.

As a consequence of learning from the prototype fabrication, many improvements are being carried out, including placing markers directly at node locations, a reduction in the number of components (such as nuts and printed spacers) and measurement points. This research also showed the potential in using a standard model, vision and control algorithms and equipment to deal with complex, highly indeterminate, kinematic structural systems such as cable structures, stadia roof, cable-stayed bridges and tensegrity structures.

References

[1] D. Veenendaal, P. Block, Design process for prototype concrete shells using a hybrid cable-net and fabric formwork, Eng. Struct. 75 (2014) 39–50.
[2] D. Veenendaal, M. West, P. Block, History and overview of fabric formwork: using fabrics for concrete casting, Struct. Concr. 12 (3) (2011) 164–177.

[3] E.D. Bolster, H. Cuypers, P.V. Itterbeeck, J. Wastiels, W.P. De Wilde, Use of hypar-shell structures with textile reinforced cement matrix composites in lightweight constructions, Compos. Sci. Technol. 69 (2009) 1341–1347.

[4] J.L. Waling, B. Greszczuk, L. Experiments with thin-shell structural models, J. Am. Concr. Inst. (57-20) (1960) 413–432.

[5] R. Torsing, J. Bakker, R. Jansma, D. Veenendaal, Large-scale designs for mixed fabric and cable net formed structures, Proceedings of the 2nd International Conference on Flexible Formwork, 2012, pp. 346–355.

[6] NEST Hilo research and innovation unit 2016, https://www.empa.ch/web/nest.

[7] Z. Nagy, B. Svetozarevic, P. Jayathissa, M. Begle, J. Hofer, G. Lydon, A. Willmann, A. Schlueter, Front. Archit. Res. 5 (2) (2016) 143–156.

[8] A. Liew, D. López López, T. Van Mele, P. Block, Design, fabrication and testing of a prototype, thin-vaulted, unreinforced concrete floor, Eng. Struct. 137 (2017) 323–335.

[9] A. Groenewolt, J. Bakker, J. Hofer, Z. Nagy, A. Schlüter, Methods for modelling and analysis of bendable photovoltaic modules on irregularly curved surfaces, Int. J. Energy Environ. Eng. (2016) 1–11.

[10] D. Veenendaal, J. Bakker, P. Block, Structural design of the flexibly formed, mesh-reinforced sandwich shell roof of NEST hilo, J. Int. Assoc. Shell Spatial Struct. (2017).

[11] D. Veenendaal, M. Bezbradica, D. Novak, P. Block, Controlling the geometry and forces of hybrid cable-net and fabric formworks, Proceedings of the IASS-SLTE 2014

[12] T. Van Mele, P. Block, A novel form finding method for fabric formwork for concrete shells, J. Int. Assoc. Shell Spatial Struct. 52 (4) (2011) 217–224.

[13] S. Guillaume, B. Bürki, S. Griffet, H.M. Durand, Qdaedalus: Augmentation of Total Stations by CCD Sensor for Automated Contactless High-precision Metrology, (2012) FIG Working Week, Rome Italy.

[14] B. Bürki, S. Guillaume, Sorber, H.P.P. Oesch, Daedalus: a versatile usable digital clip-on measuring system for total stations, International Conference on Indoor Positioning and Indoor Navigation (IPIN), Zürich, 2010.

[15] S. Guillaume, J. Clerc, C. Leyder, J. Ray, M. Kistler, Contribution of the image-assisted theodolite system QDaedalus to geodetic static and dynamic deformation monitoring, 3rd Joint International Symposium on Deformation Monitoring (JISDM), Vienna Austria, 2016.

[16] S. Guillaume, C. Muller, P.H. Cattin, TRINET+, logiciel de compensation 3D version 6.1,. Mode d'emploi HEIG-VD, Yverdon Switzerland 2008.

[17] Y.R. Stürz, M. Morari, R.S. Smith, Sequential quadratic programming for the control of an architectural cable net geometry, Proceedings of the American Control Conference, 2016, pp. 3503–3508.

[18] M.S. Lobo, L. Vandenberghe, S. Boyd, H. Le-Bret, Applications of second-order cone programming, 284 (1998).

[19] J. Nocedal, S.J. Wright, Numerical optimization, Springer Series in Operations Research and Financial Engineering, 2nd ed., (2006).